# Figures and figure supplements

Dichotomy between extracellular signatures of active dendritic chemical synapses and gap junctions

**Richa Sirmaur and Rishikesh Narayanan.**

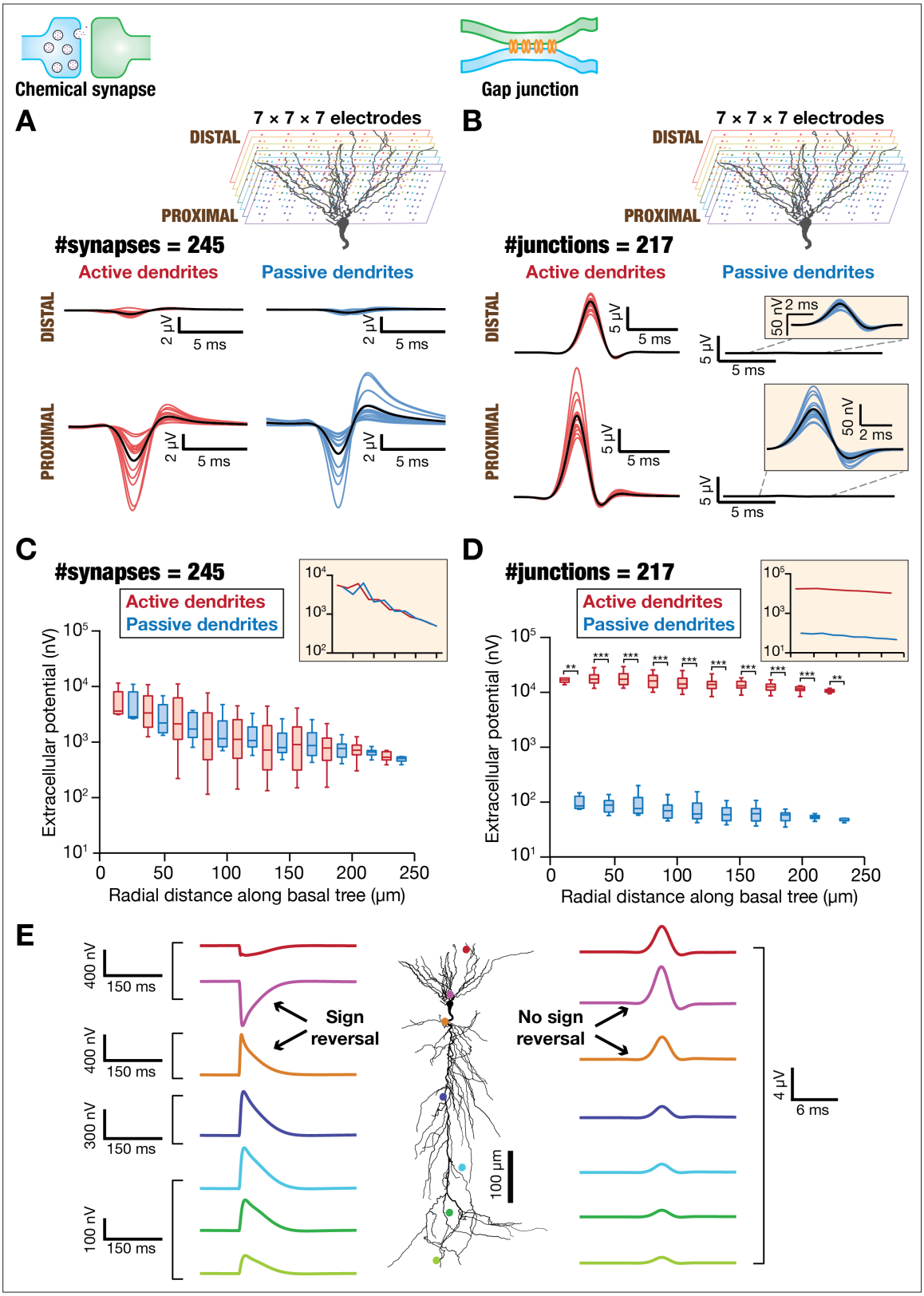


**Figure 1.** Contrasting extracellular signatures associated with active dendritic chemical synapses *vs.* gap junctions receiving synchronous inputs. (**A**) *Top*, 3D electrode setup representing 7×7×7 (343 in total) electrode array spanning the basal dendrites of a CA1 pyramidal neuron morphology. Although the entire morphology was used for simulations spanning the apical and basal dendrites, the depiction here is restricted to the basal dendrites to emphasize electrode locations. *Bottom*, field potential traces from electrodes at proximal (15 traces representing different locations within 50–

*Figure 1 continued on next page*

*Figure 1 continued*

100 μm) and distal (21 traces representing different locations within 190–300 μm) locations along the somato-basal axis, when dendrites were active (*left*) or passive (*right*). Black traces depict the respective average trace across all distal or proximal locations. The 245 chemical synapses ($N_{\mathrm{syn}} = 245$) which were randomly dispersed across the basal dendrites received synchronous inputs. (**B**) Same as **A**, but for external inputs arriving through gap junctions. The number of gap junctions $N_{\mathrm{jun}} = 217$. (**C**) Amplitudes of negative deflection of field potentials for all 343 electrodes, plotted as functions of radial distance of the electrode from the soma, for active and passive dendritic models receiving synchronous inputs through chemical synapses ($N_{\mathrm{syn}} = 245$). Inset shows plot of median field potential amplitude values as a function of distance for both active and passive dendritic configurations. (**D**) Same as **C**, but amplitudes of positive deflections in extracellular potentials associated with inputs arriving through gap junctions. The number of gap junctions $N_{\mathrm{jun}} = 217$. Comparison of active *vs.* passive dendritic configurations in (**C–D**): *$p$<0.05, *$p$<0.01, ***$p$<0.001, Wilcoxon rank-sum test. (**E**) Extracellular electrodes were placed across the entire span of the neuron (active dendrites with no sodium) instead of being confined to the basal dendritic span (panels **A–D**), with all parameters set identical to panels (**A–D**). A flip in the sign of the extracellular potentials may be noted for synchronous stimulation with chemical synapses (*Left*), but not with stimulation with gap junctions (*Right*).

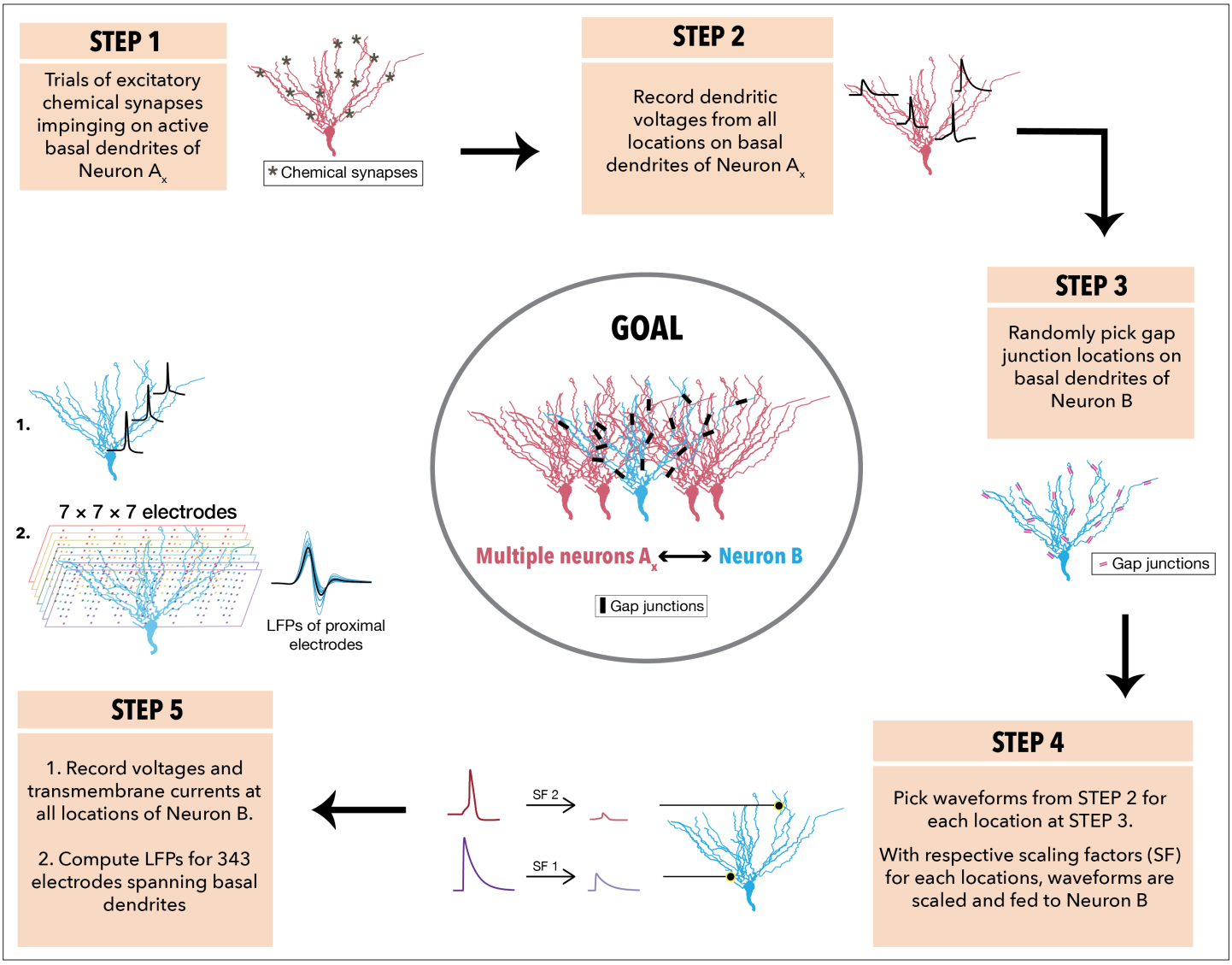


**Figure 1—figure supplement 1.** Methodology for assessing extracellular signatures of gap junctional synapses onto a neuron. Extracellular potentials were assessed for gap junctional inputs onto the dendrites of Neuron B. To implement this, several neurons $A_x$ were considered to make gap junctional connections onto Neuron B (circle in the center named 'Goal'). **Step 1**: Each neuron $A_x$ was considered to receive chemical synaptic inputs located on their active dendrites. There were no chemical synapses on Neuron B. **Step 2**: Dendritic voltages were recorded from all compartments. Depending on strength and location, these waveforms could take the form of synaptic potentials, dendritic spikes, or backpropagating action potentials. Several trials of such recordings were performed with variable localization of chemical synapses, each constituting one of the $A_x$ neuron. **Step 3**: Randomly pick gap junctional locations on Neuron B where one of the $A_x$ neurons will make contact. **Step 4**: Pick one of the waveforms from one of the trials from Step 2 and associate that waveform with one of the locations picked in Step 3. Scale the waveform (chosen from Step 2) using a location-dependent scaling factor (which represents the strength of the gap junction at the location picked in Step 3), convert the waveform into a current, and inject the current into the location chosen in Step 3. Repeat this process for all gap junctions on Neuron B. This step configures all gap junctions in Neuron B and the kind of inputs that they receive from each of the $A_x$ neurons. **Step 5**: Record voltages and transmembrane currents from all locations of Neuron B. Use the transmembrane currents from all compartments to compute potentials at all the 7×7×7 extracellular electrodes.

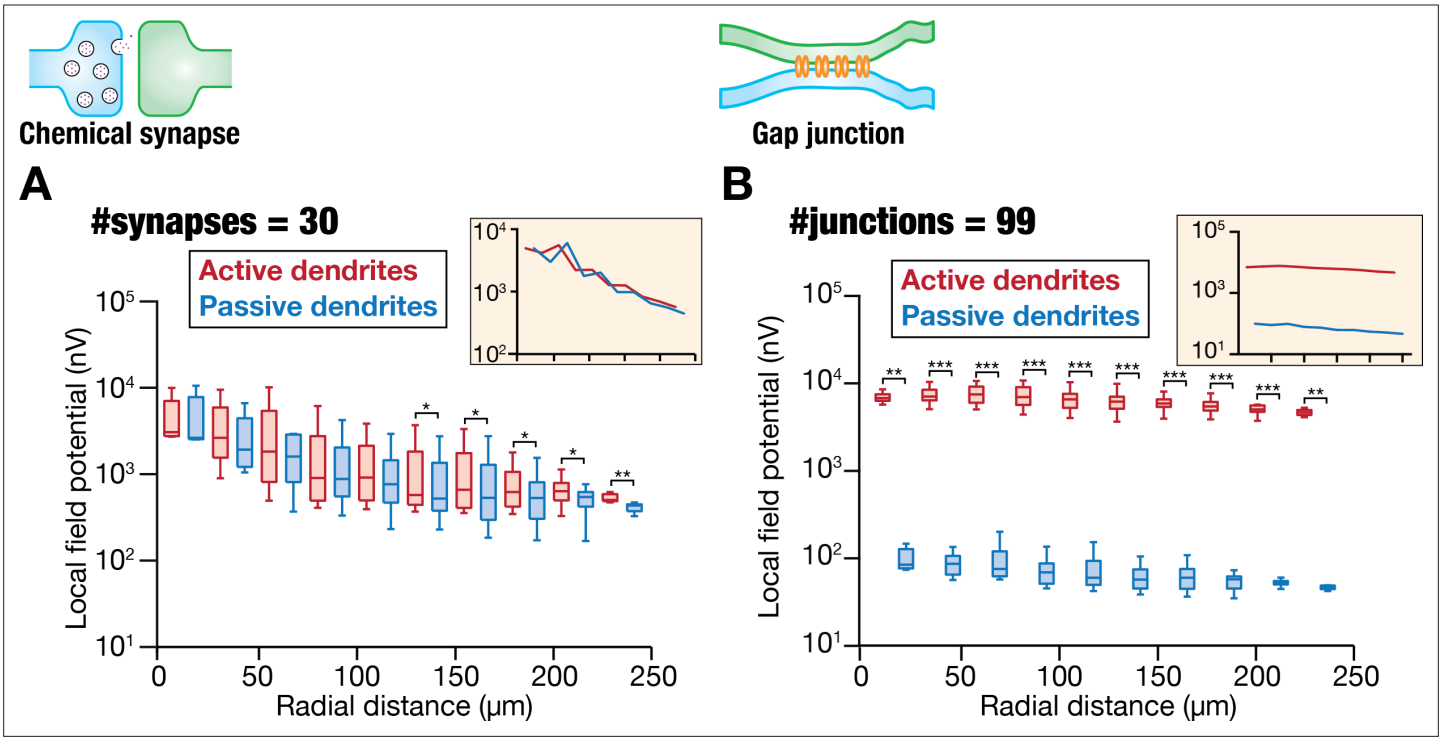


**Figure 1—figure supplement 2.** Extracellular signatures associated with active dendritic chemical synapses *vs.* gap junctions receiving synchronous inputs. (**A**) Amplitudes of negative deflection of field potentials for all 343 electrodes, plotted as functions of radial distance of the electrode from the soma, for active and passive dendritic models receiving synchronous inputs through chemical synapses ($N_{\mathrm{syn}} = 30$). Inset shows plot of median field potential amplitude values as a function of distance for both active and passive dendritic configurations. (**B**) Same as **A**, but for external inputs arriving through gap junctions. The number of gap junctions $N_{\mathrm{jun}} = 99$. Comparison of active *vs.* passive dendritic configurations in (**A–B**): *$p$<0.05, **$p$<0.01, ***$p$<0.001, Wilcoxon rank-sum test.

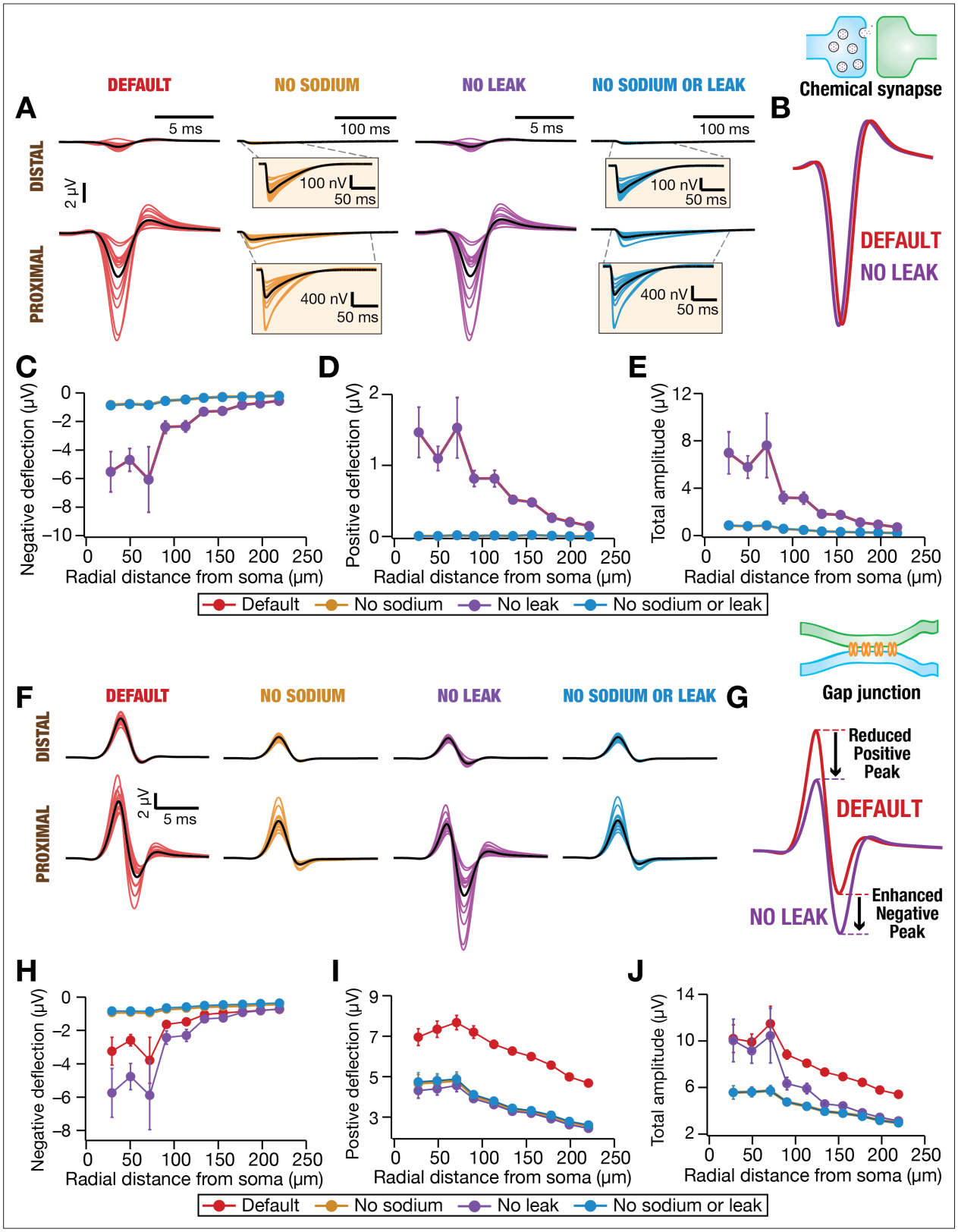


**Figure 2.** Differential polarity of field potentials associated with synchronous inputs through chemical synapses *vs.* dendro-dendritic gap junctions on active dendrites. (**A**) Extracellular potentials from electrodes at proximal (15 colored traces represent different locations within 50–100 μm) and distal (21 colored traces represent different locations within 190–300 μm) locations along the somato-basal axis. Shown are traces for default (where all components were present), no sodium, no leak, and no sodium or leak scenarios for active dendritic structures. Black traces in each scenario depict the

*Figure 2 continued on next page*

*Figure 2 continued*

respective average trace across all distal or proximal locations. The 245 chemical synapses ($N_{\mathrm{syn}} = 245$) which were randomly dispersed across the basal dendrites received synchronous inputs. (**B**) Zoomed example trace (from a proximal electrode at 54 μm from soma) showing the impact of leak channels in shaping the extracellular potentials associated with active dendritic structures with (Default) and without leak channels (No leak). (**C–E**) Mean and SEM of the amplitudes of negative deflection (**C**), positive deflection (**D**), and the total peak-to-peak amplitude (**E**) of the extracellular potentials, plotted as functions of radial distance of electrode location, for default, no sodium, no leak, and no sodium or leak scenarios for active dendritic structures. (**F–J**) Same as panels (**A–E**) but for active dendritic structures receiving synchronous inputs through dendro-dendritic gap junctions ($N_{\mathrm{jun}} = 99$).

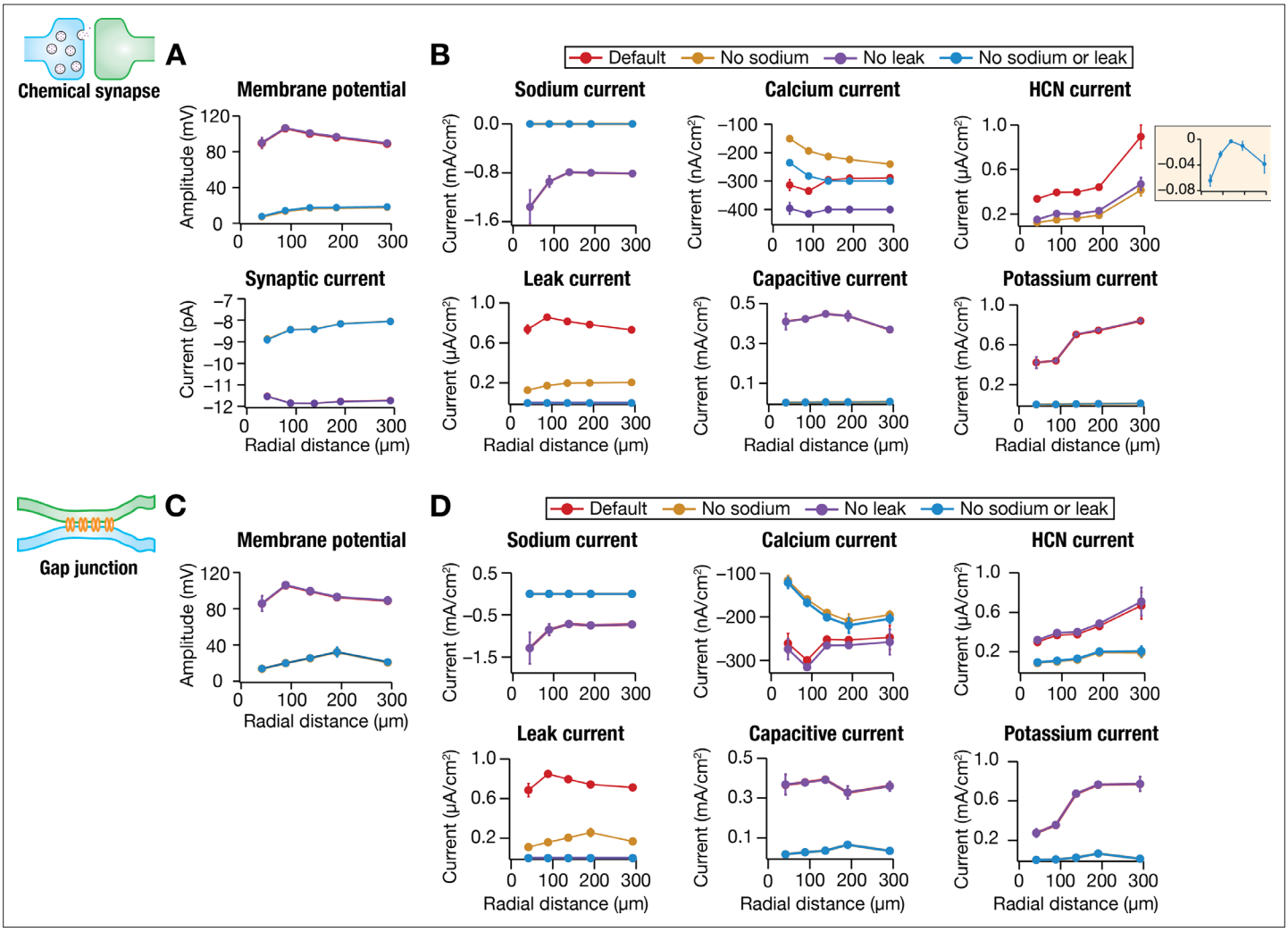


**Figure 3.** Ionic basis of the differential contributions of transmembrane currents to field potentials associated with synchronous inputs arriving through chemical synapses *vs.* gap junctions on active dendrites. (**A**) Mean and SEM of peak membrane voltages (*top*) and peak synaptic currents (*bottom*) from across somato-basal locations recorded intracellularly for all 4 model configurations. The four different model configurations shown are the default active model, and the active models where sodium channels, leak channels, or both sodium and leak channels were absent. It may be noted that there were no action potentials or dendritic spikes when there were no sodium channels in the models. The dependence of synaptic current on the membrane potential, acting as the driving force, may also be noted. (**B**) Mean and SEM of peak values of transmembrane sodium, calcium (*T*-type, *L*-type, *R*-type, and *N*-type), HCN, leak, capacitive, and potassium (*A*-type, delayed rectifier, and *M*-type) currents for different active models receiving synchronous inputs through chemical synapses, plotted as functions of radial distance from soma for all 4 model configurations. (**C–D**) Same as panels (**A–B**) but with different configurations of active models receiving synchronous inputs through gap junctions. There are no synaptic currents plotted here as there are no transmembrane synaptic currents associated with gap junctions.

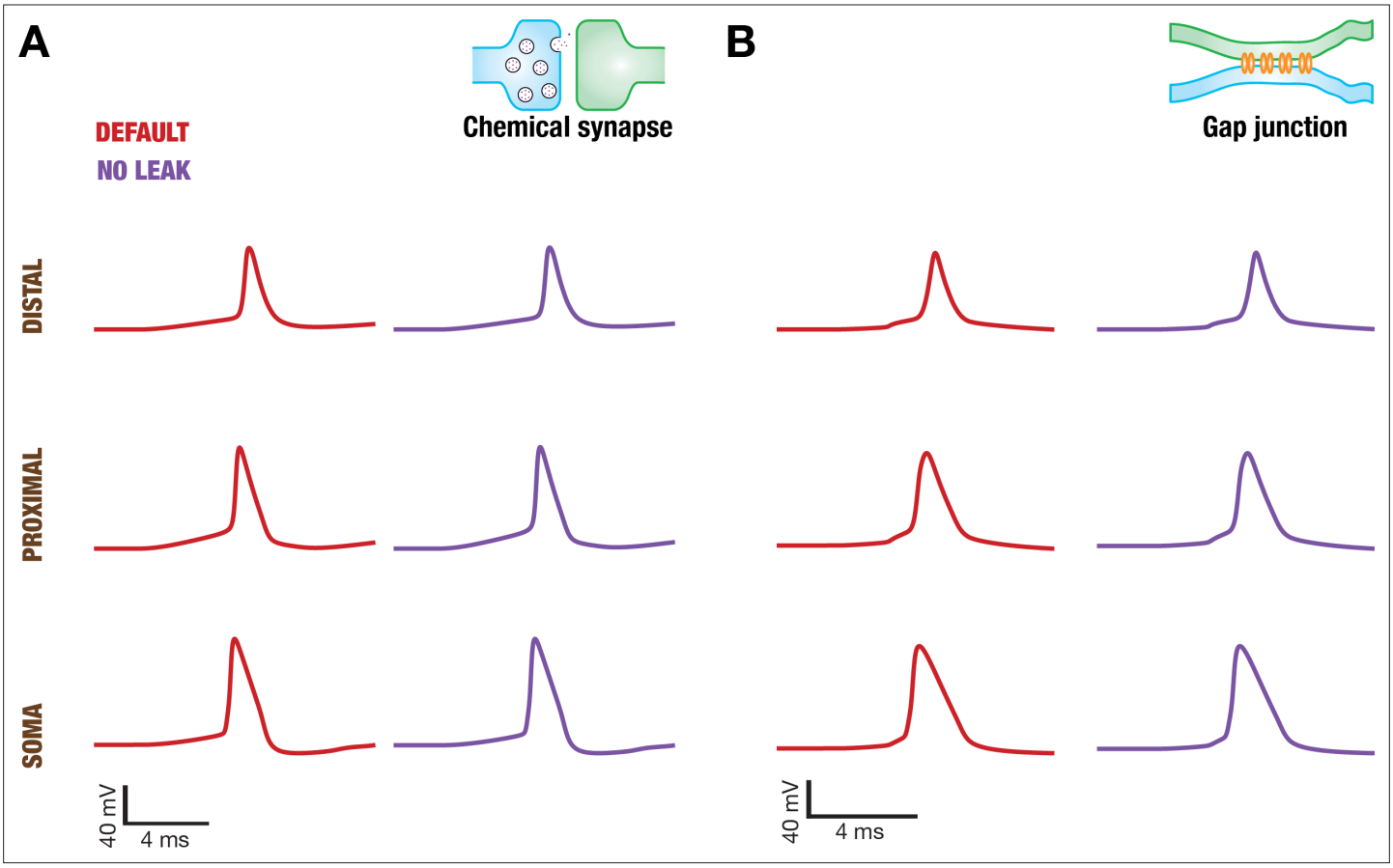


**Figure 3—figure supplement 1.** Intracellular potentials associated with active dendritic chemical synapses *vs.* gap junctions receiving synchronous inputs. (**A**) Intracellular responses recorded at soma *(Row 1)*, proximal (100 µm; *Row 2*), and distal (200 µm; *Row 3*) dendritic locations along the somato-basal axis. Shown are the traces for default *(Column 1)* and no leak *(Column 2)* scenarios for active dendritic structures receiving synchronous inputs via chemical synapses. (**B**) Same as panel *A* but with active dendrites receiving synchronous inputs through gap junctions.

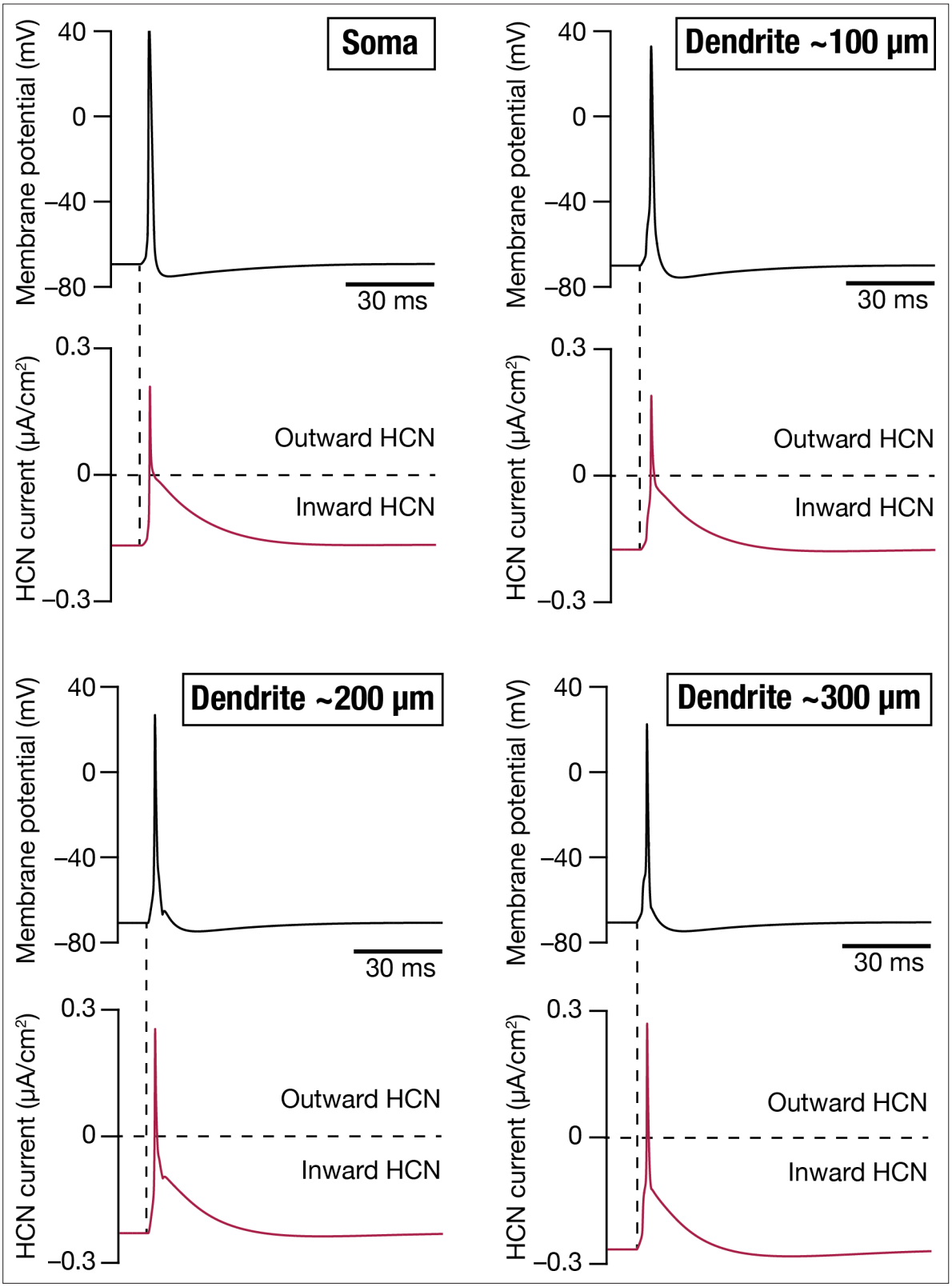


**Figure 3—figure supplement 2.** Outward transmembrane HCN currents recorded at different somatic and active dendritic compartments receiving synchronous inputs through gap junctions. Intracellular voltages (black) and current through HCN channels (red) plotted for different somatic and dendritic (shown are distances from the soma) compartments (total duration: 110 ms). Vertical dashed lines represent the onset of synchronous inputs through gap junctions and the horizontal lines represent the transition point from inward to outward current through the HCN channels. In each case,

*Figure 3—figure supplement 2 continued on next page*

*Figure 3—figure supplement 2 continued*

it may be noted that under resting conditions, there is an inward (negative) resting HCN current. With the onset of synchronous stimulus, the sharp transition in voltage towards eliciting a spike alters the driving force for this resting HCN conductance. As the voltage in the compartment reaches beyond the HCN reversal potential (–30 mV), the current reverses direction to manifest an outward (positive) current through HCN channels. Thus, the resting HCN conductance combined with a sharp transition in voltage that crosses the HCN-channel reversal potential together yield an outward HCN current.

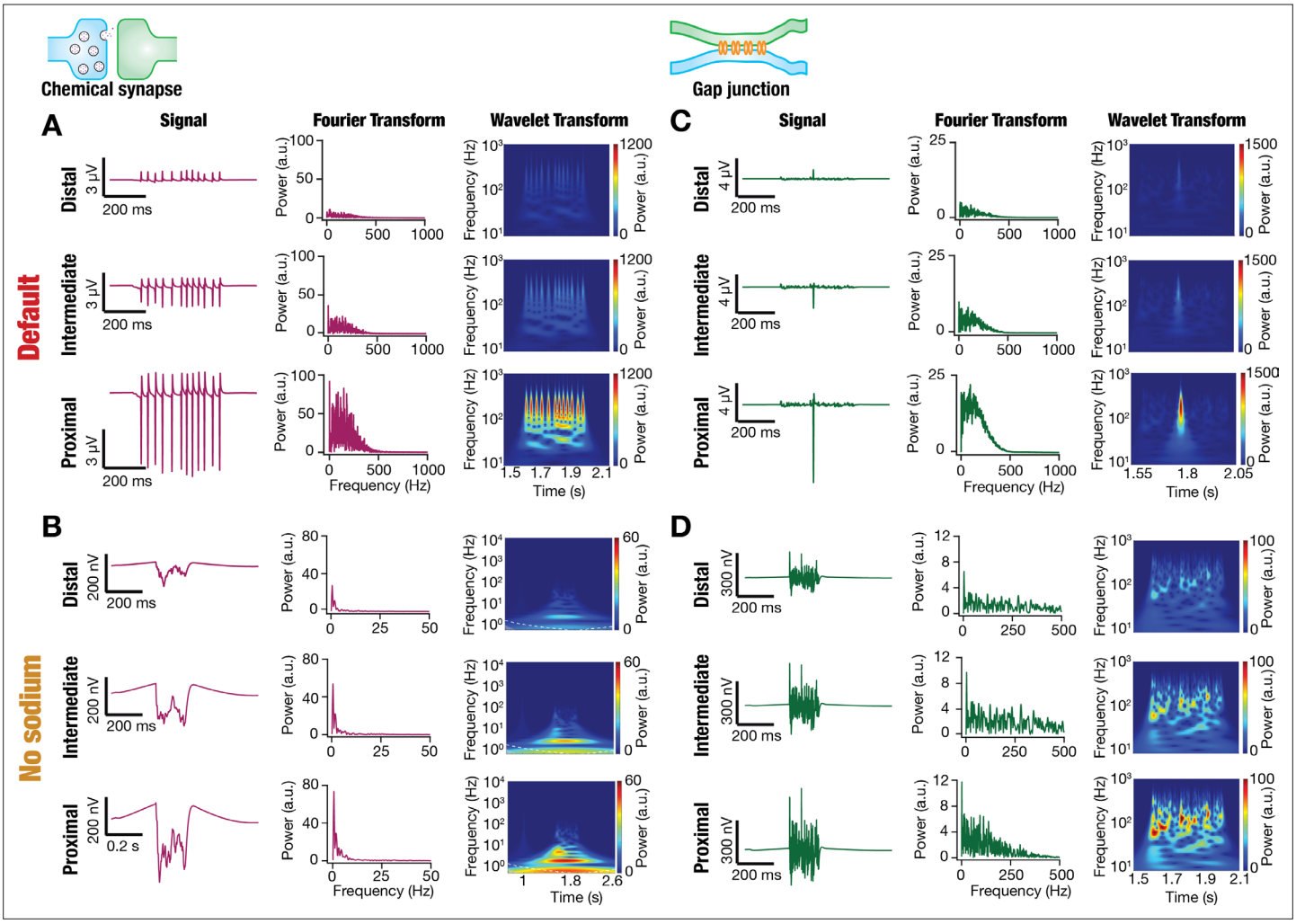


**Figure 4.** Differential spatiotemporal structure of field potentials associated with active dendrites receiving low-frequency random inputs through chemical synapses *vs.* gap junctions. (**A**) Distance-wise local field potential (LFP) responses to low-frequency random inputs (LFRI) impinging on active dendrites through chemical synapses. *Rows 1–3:* LFP data from electrodes located at a distal (~152 μm; *Row 1*), intermediate (~97 μm; *Row 2*), and proximal (~55 μm) locations with reference to their radial distance from the soma. *Column 1:* time-domain signal. *Column 2:* Fourier transform of the signal shown in *Column 1. Column 3:* spectrogram of the signal shown in *Column 1* computed using wavelet transform. (**B**) Same as panel (**A**) but for active model lacking sodium conductance. (**C–D**) Same as panels (**A–B**), except low-frequency random inputs impinged onto active dendrites through gap junctions.

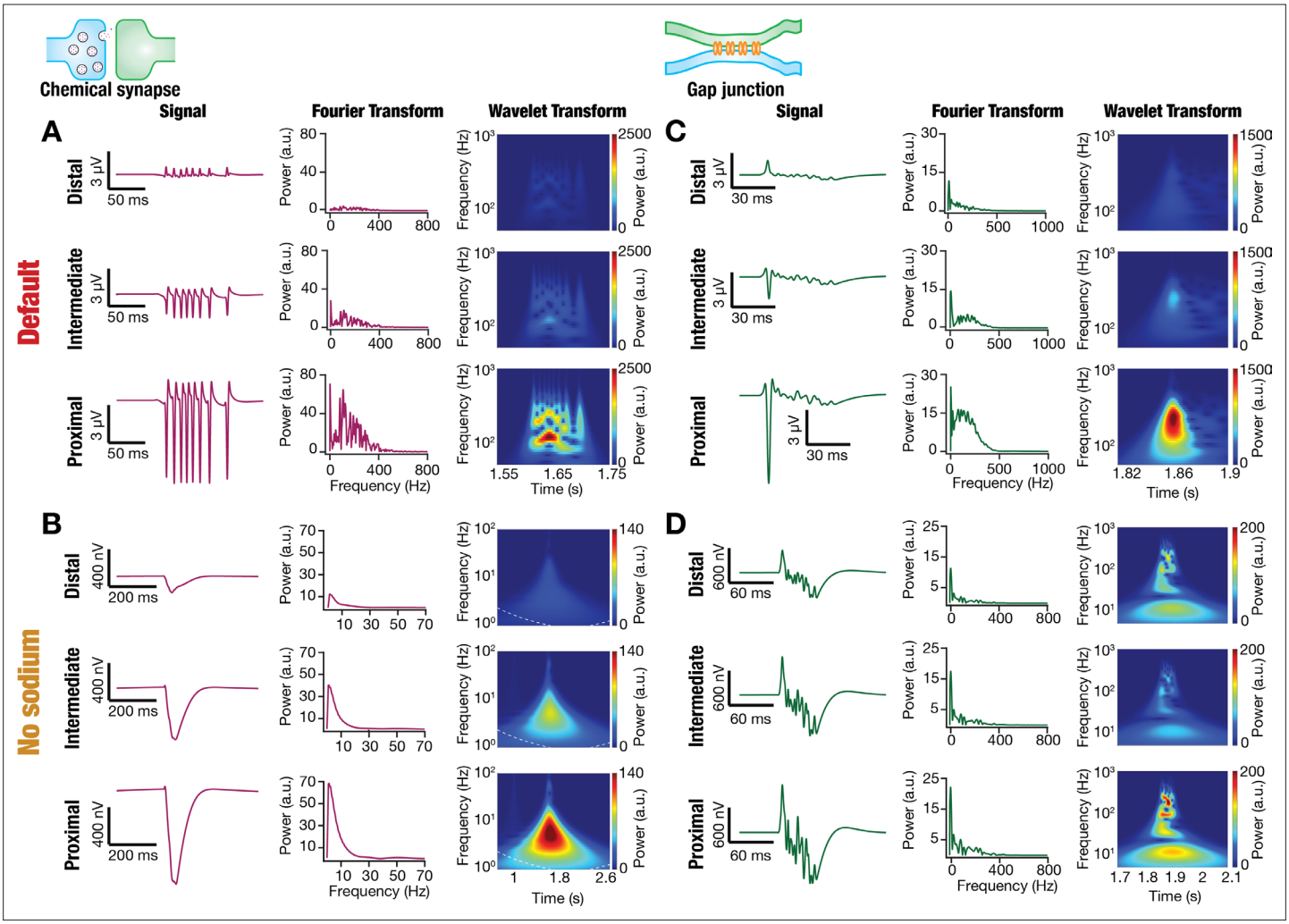


**Figure 4—figure supplement 1.** Differential spatiotemporal structure of field potentials associated with active dendrites receiving high-frequency random inputs through chemical synapses *vs.* gap junctions. (**A**) Distance-wise local field potential (LFP) responses to high-frequency random inputs (HFRI) impinging onto active dendrites through chemical synapses. *Rows 1–3:* LFP data from electrodes located at a distal (~152 μm; *Row 1*), intermediate (~97 μm; *Row 2*), and proximal (~55 μm; *Row 3*) locations with reference to their radial distance from the soma. *Column 1:* time-domain signal. *Column 2:* Fourier transform of the signal shown in *Column 1*. *Column 3:* spectrogram of the signal shown in *Column 1* computed using wavelet transform. (**B**) Same as panel (**A**) but for active model lacking sodium conductance. (**C–D**) Same as panels (**A–B**), except high-frequency random inputs impinged onto active dendrites through gap junctions.

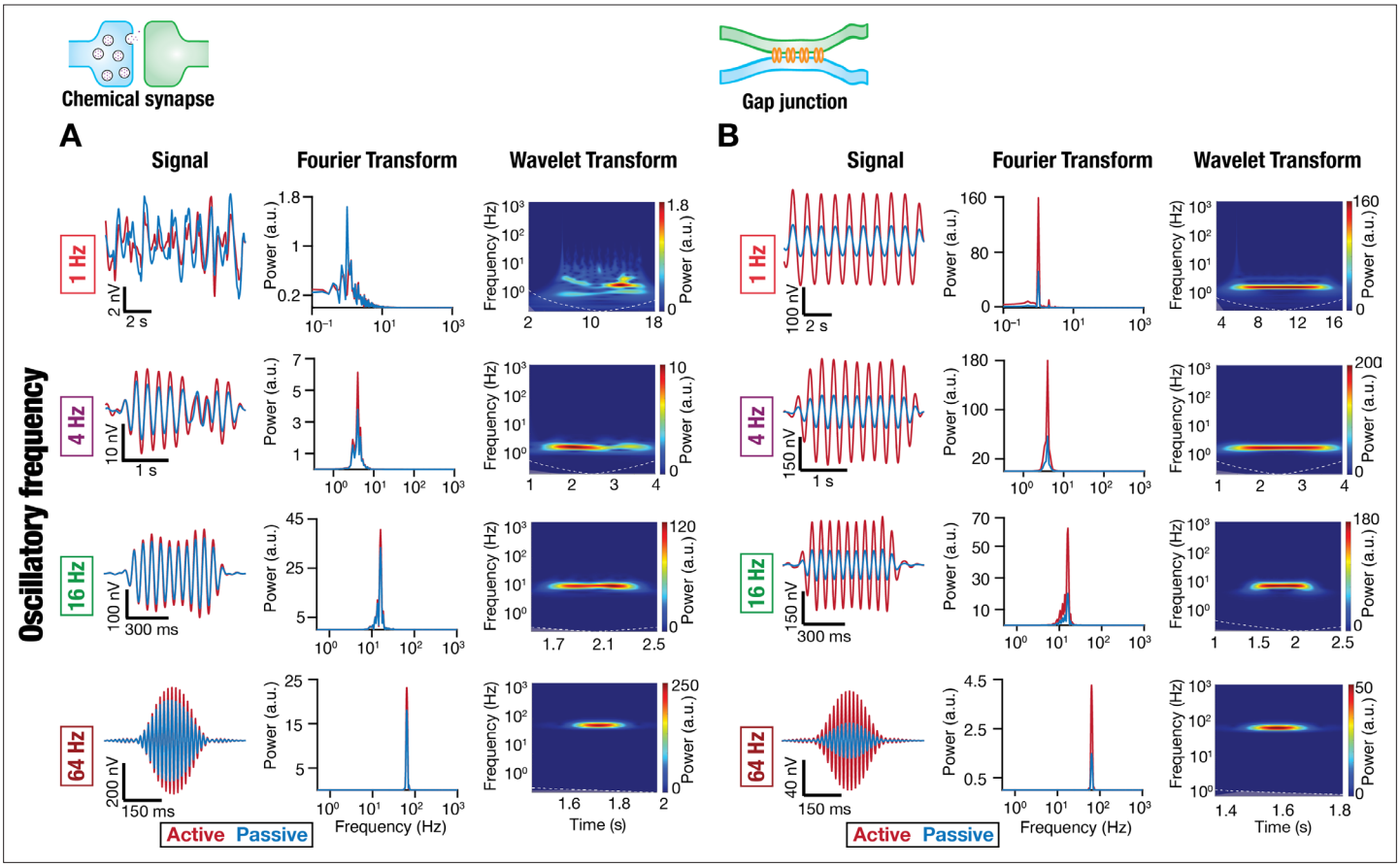


**Figure 5.** Dominance of specific oscillatory bands in field potentials depended on whether inputs onto active dendrites were received through chemical synapses or gap junctions. (**A**) Example local field potential (LFP) responses to rhythmic inputs at different (1–64 Hz) frequencies and their spectral signatures, shown for simulations performed with active or passive basal dendrites receiving rhythmic inputs through chemical synapses. Each row shows the filtered LFP signal at an electrode placed ~97 µm from the soma, the Fourier power spectrum, and the wavelet spectrogram for the LFP signal. Different rows depict different input frequency values for the rhythmic input (1 Hz, 4 Hz, 16 Hz, and 64 Hz). (**B**) Same as (**A**) but for the rhythmic inputs impinging on basal dendrites at different frequencies through gap junctions. All simulations depicted here were performed in the absence of sodium channels to avoid spiking.

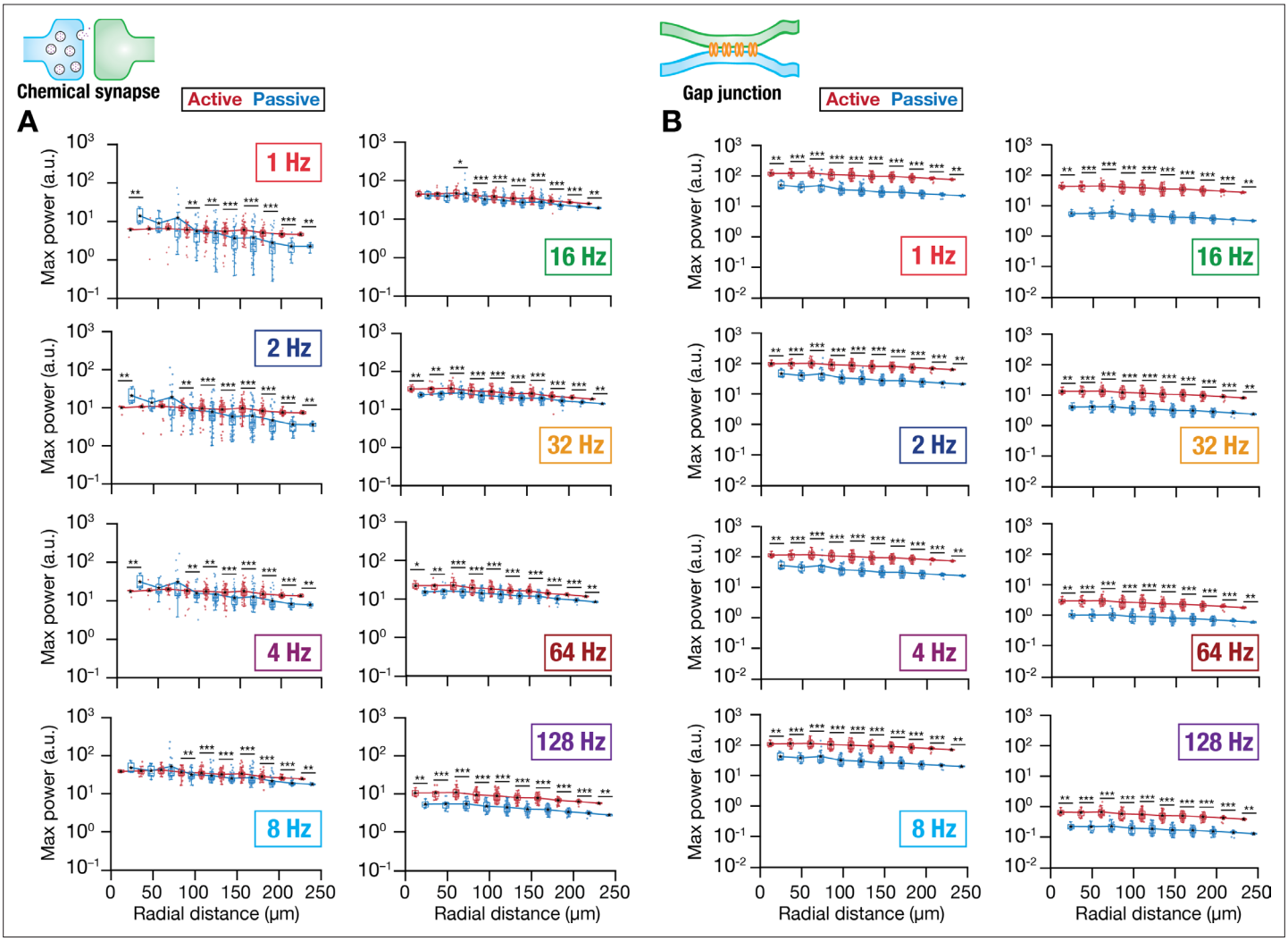


**Figure 6.** Distance-dependence of spectral power in specific bands of field potentials associated with active dendrites receiving rhythmic inputs through chemical synapses or gap junctions. (**A**) Maximum power in local field potential (LFP) responses associated with rhythmic inputs at different (1–128 Hz) frequencies, shown for simulations performed with active or passive basal dendrites receiving these rhythmic inputs through chemical synapses. All electrodes at specific radial distances are depicted for each scenario. The frequency of the rhythmic input is highlighted in each panel. (**B**) Same as (**A**) but for the rhythmic inputs impinging on basal dendrites at different frequencies through gap junctions. Across all plots, lines connect the respective median values (represented by black stars). All simulations depicted here were performed in the absence of sodium channels to avoid spiking. *$p$<0.05, **$p$<0.01, ***$p$<0.001 (Wilcoxon rank-sum test).

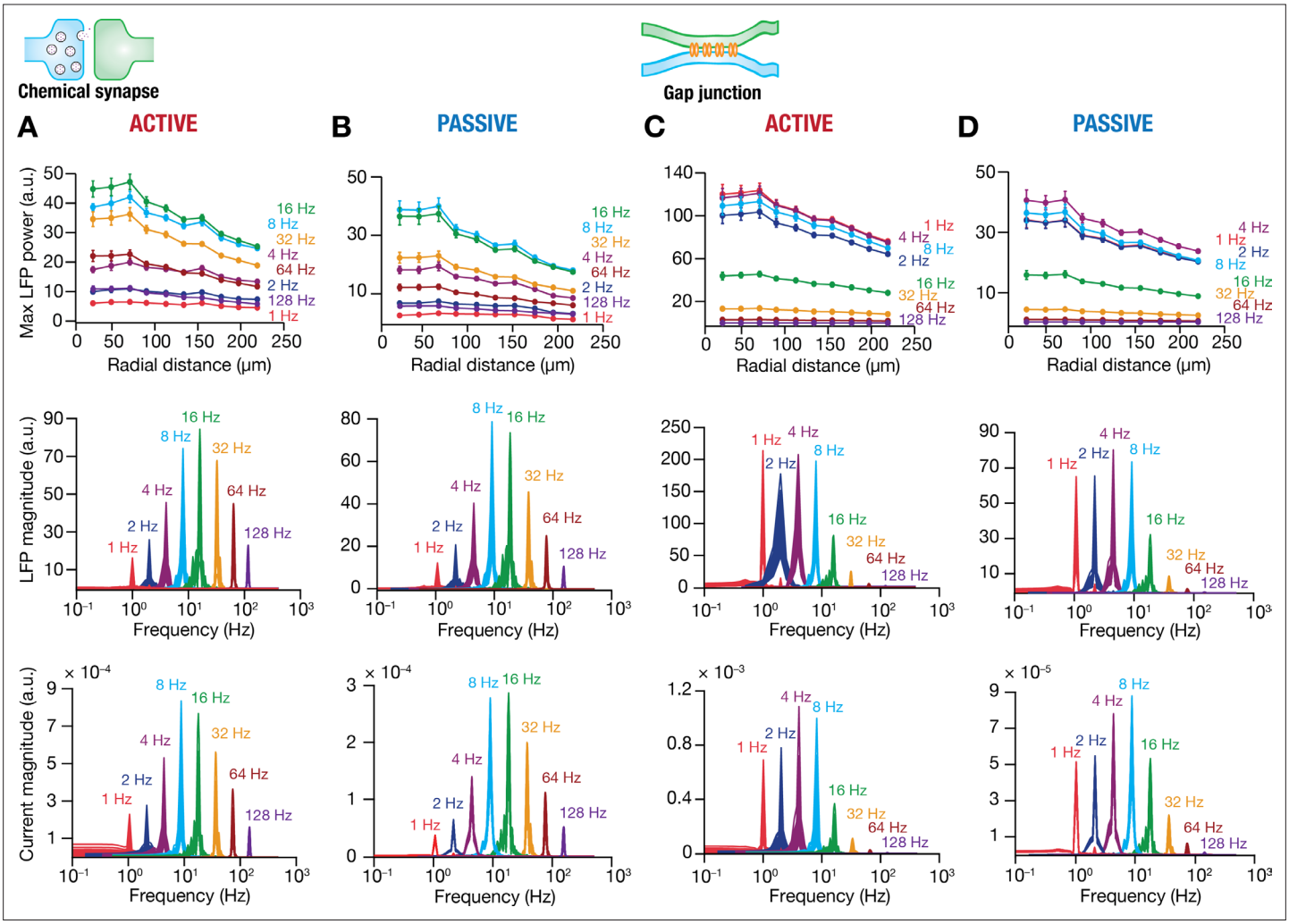


**Figure 7.** Transmembrane currents driven by voltage responses mediate the differential emphasis of specific oscillatory bands in field potentials associated with chemical synapses *vs.* gap junctions on active dendrites. (**A**) *Row 1:* Distance-dependent maximal power of local field potentials recorded at different electrodes (shown as mean and SEM) associated with neuronal response to rhythmic inputs at different frequencies impinging on the active basal dendritic model through chemical synapses. *Row 2:* Fourier power spectra for all field potentials at different frequencies of the rhythmic inputs. Each trace for a given frequency represents different electrodes. *Row 3:* Fourier spectra of the filtered total transmembrane current for each frequency of rhythmic inputs, from each basal dendritic compartment. (**B**) Same as panel **A**, but for simulations performed with passive dendrites. (**C–D**) Same as (**A–B**), but with rhythmic inputs coming through gap junctions. All simulations depicted here were performed in the absence of sodium channels to avoid spiking.

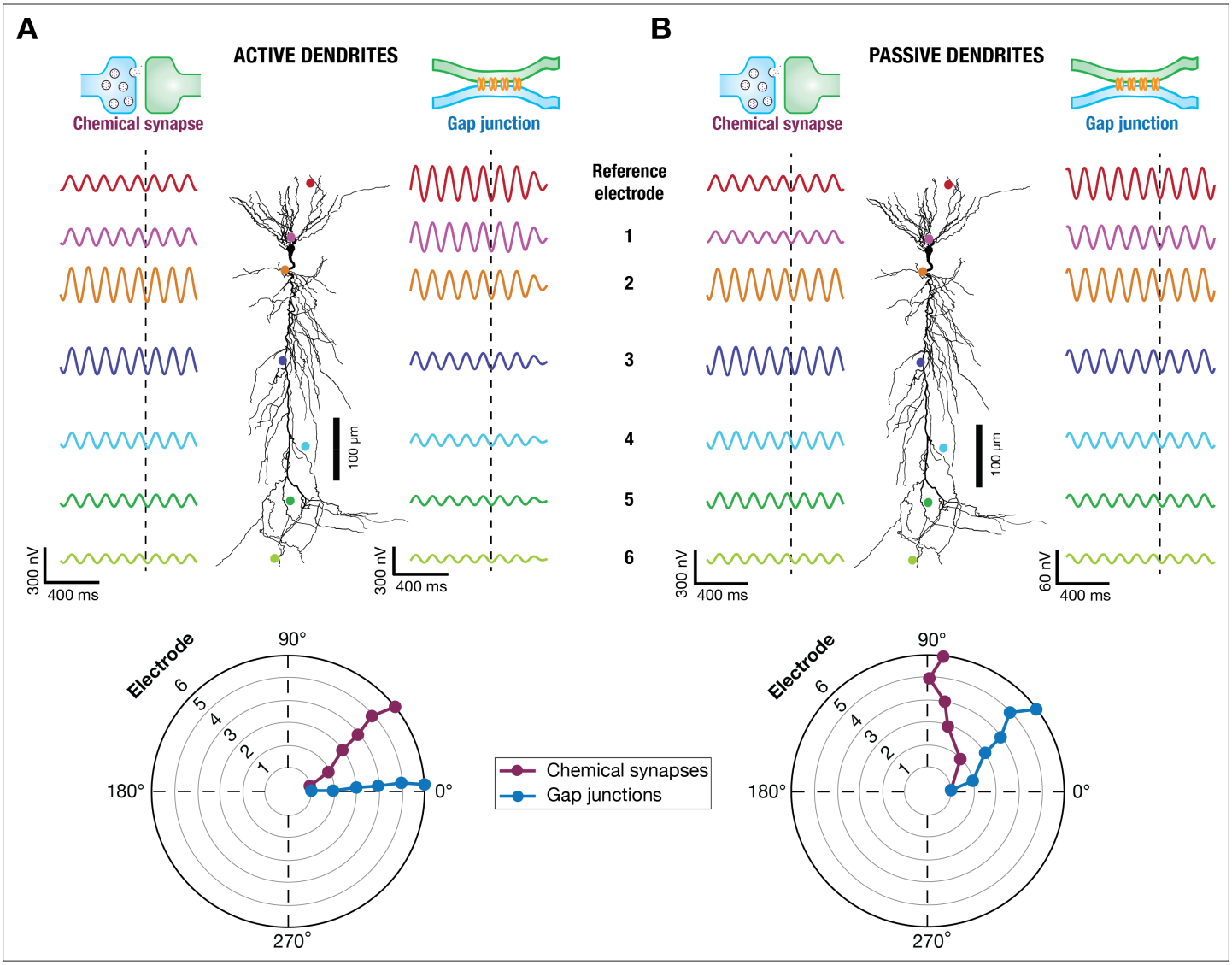


**Figure 7—figure supplement 1.** Somatic intracellular voltage–local field potential (LFP) phase relationship associated with active dendrites receiving rhythmic inputs at various frequencies through chemical synapses *vs.* gap junctions in models with no sodium channels. (**A**) *Top*, Extracellular potentials simultaneously recorded from electrodes that were placed across the entire span of the neuron when active dendrites received rhythmic inputs at 8 Hz through chemical synapses (*left*) or through gap junctions (*right*). 2D projections of the different electrodes and the neuronal morphology are depicted in the center. The electrode at the distal-most basal location was treated as the reference electrode to compute phase differences in the extracellular potentials observed across different electrodes. The dashed line marks a trough of the oscillatory pattern observed in the extracellular potential associated with the reference electrode. *Bottom,* phase differences, computed through cross-correlation analysis, between the extracellular potentials recorded from the reference electrode and those from electrodes 1–6, in scenarios where rhythmic inputs arrived through chemical synapses or gap junctions. (**B**) Same as panel A, but for models where the dendrites were passive.

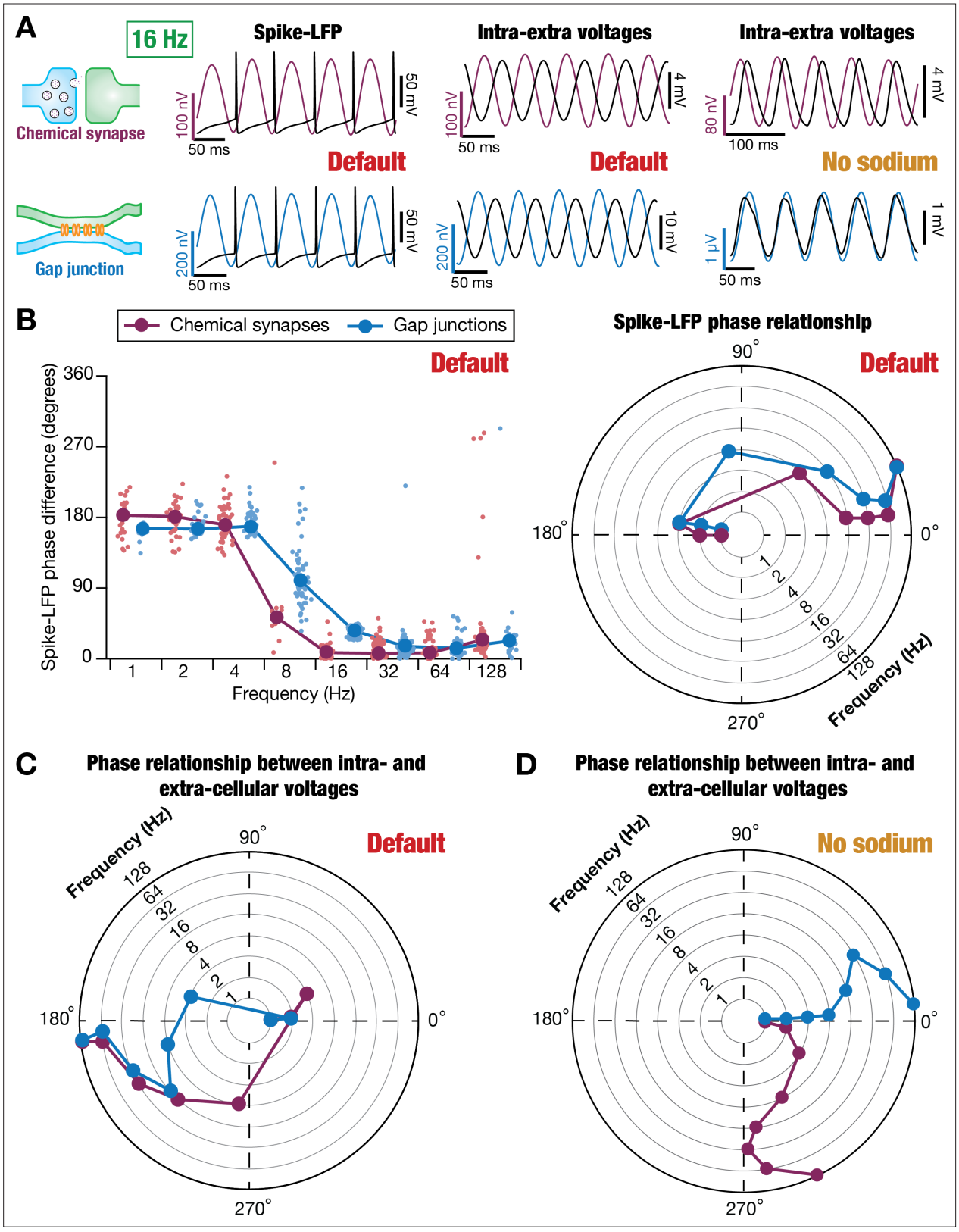


**Figure 8.** Differential phase relationship between local field potentials and spikes associated with rhythmic inputs through chemical synapses *vs.* gap junctions on active dendrites. (**A**) Example local field potential (LFP) traces (color coded based on whether they are associated with chemical synapses in dark pink or gap junctions in blue) and simultaneously recorded intracellular somatic voltage traces (black) for neurons receiving rhythmic inputs through chemical synapses (*top*) or gap junctions (*bottom*). Shown are traces with default model configuration where all channels were intact (*left*), traces where

*Figure 8 continued on next page*

*Figure 8 continued*

the intracellular traces were filtered to the respective band (*middle*), and extracellular/intracellular traces obtained in the absence of sodium channels (*right*). (**B**) *Left,* spike phase with reference to local field potentials for each spike (lighter circles) for oscillatory inputs at different frequencies impinging on active dendrites through chemical synapses *vs.* gap junctions. Dark-colored circles represent the median values at each frequency for the respective group. *Right,* polar version of the plot showing the median of spike-LFP phases over five trials for rhythmic inputs at different frequencies through chemical synapses and gap junctions. The different frequencies are represented along the concentric circles and the corresponding spike-LFP phase values are plotted along the angular axis. (**C**) Polar plot with the median of phases obtained from cross-correlation of *filtered* intracellular potential and corresponding LFP traces at respective frequencies over all trials. These plots were derived from the same intracellular traces as in panel *A* but represent phase differences between extracellular traces and the entire filtered intracellular voltage trace. (**D**) Polar plot of phases obtained from cross-correlation between intracellular potential (without sodium conductance) and corresponding LFP traces when oscillatory inputs were presented through chemical synapses or gap junctions.

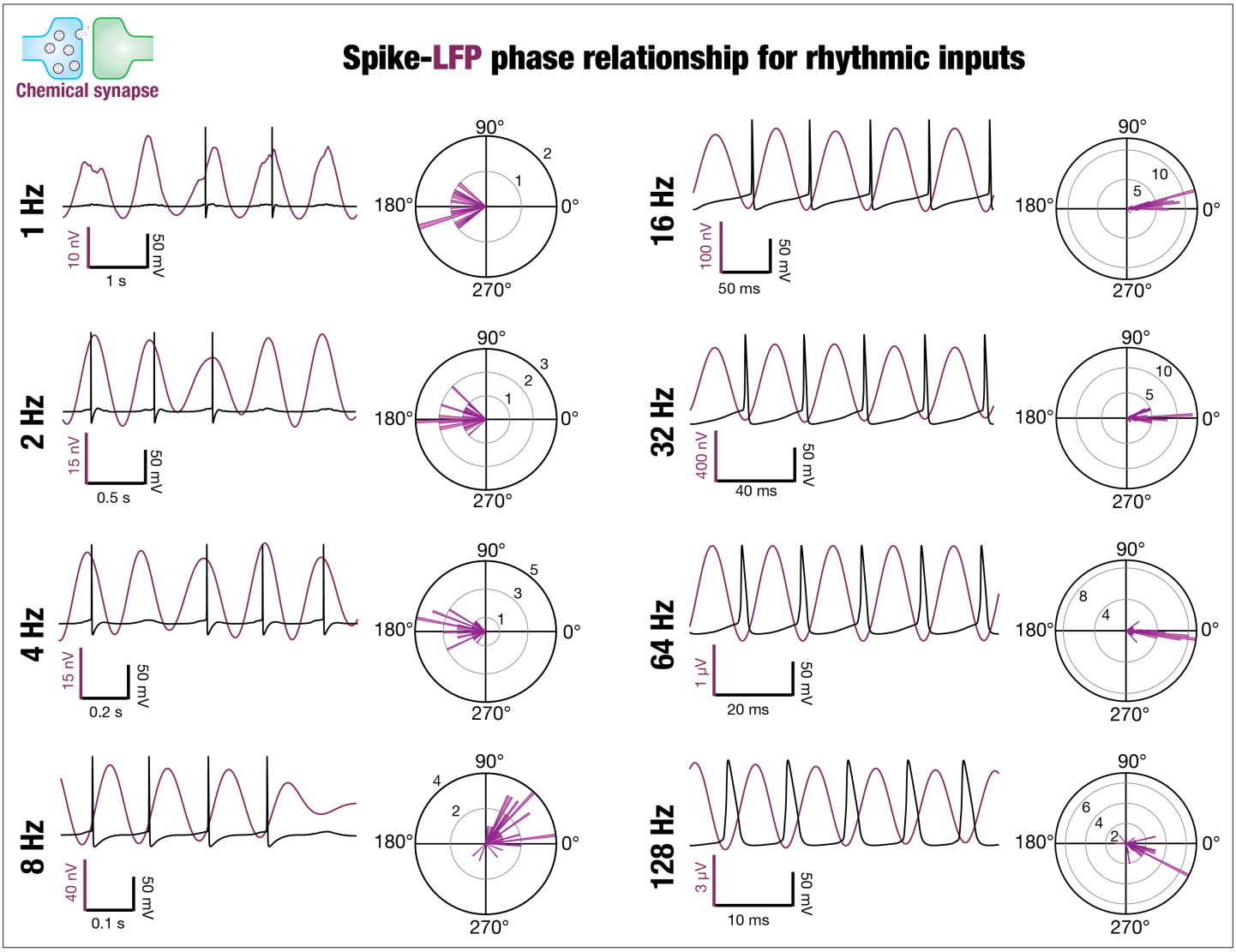


**Figure 8—figure supplement 1.** Somatic spike–local field potential (LFP) phase relationship associated with active dendrites receiving rhythmic inputs at various frequencies through chemical synapses. Phase difference between somatic spikes and corresponding extracellular potentials at different frequencies (1–128 Hz). Note that there can be traces where spikes were not observed in all cycles. The following organization is used for each of the eight frequencies. *Column 1:* Example traces of a few cycles each of intracellular potential with spikes (black) and corresponding LFP (magenta). *Column 2:* Polar plots showing the phase difference between spikes and LFPs for different trials, with 0° indicating that the spike occurred at the trough of the LFP.

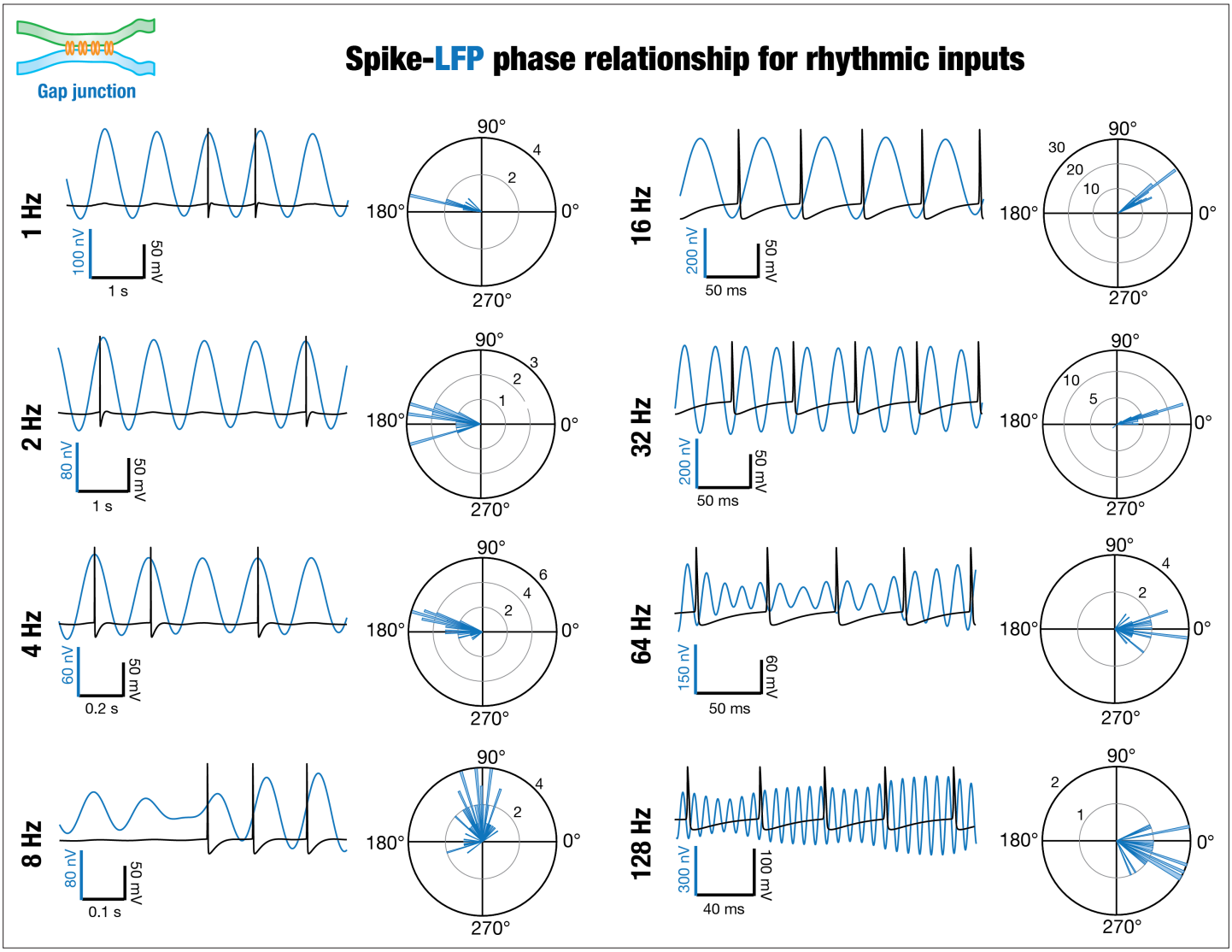


**Figure 8—figure supplement 2.** Somatic spike–local field potential (LFP) phase relationship associated with active dendrites receiving rhythmic inputs at various frequencies through gap junctions. Phase difference between somatic spikes and corresponding extracellular potentials at different frequencies (1–128 Hz). Note that there can be traces where spikes were not observed in all cycles. The following organization is used for each of the eight frequencies. *Column 1:* Example traces of a few cycles each of intracellular potential with spikes (black) and corresponding LFP (blue). *Column 2:* Polar plots showing the phase difference between spikes and LFPs, with 0° indicating that the spike occurred at the trough of the LFP.

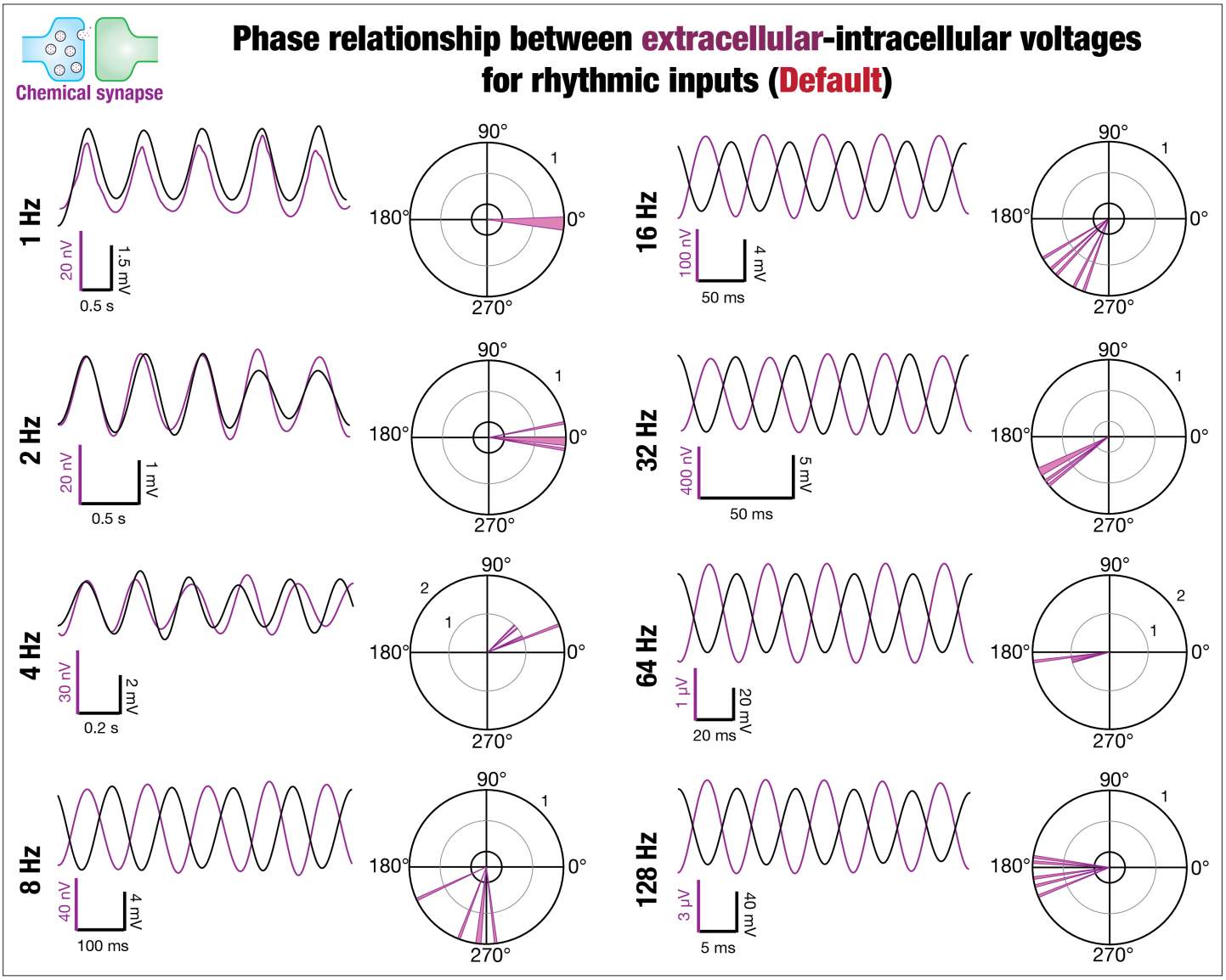


**Figure 8—figure supplement 3.** Somatic intracellular voltage–local field potential (LFP) phase relationship associated with active dendrites receiving rhythmic inputs at various frequencies through chemical synapses. Phase difference between filtered somatic intracellular potentials (from ***Figure 7—figure supplement 1***) and corresponding extracellular potentials at different frequencies (1–128 Hz). The following organization is used for each of the eight frequencies. *Column 1:* Example traces of five cycles each of intracellular potential (black) and corresponding LFP (magenta). *Column 2:* Polar plots showing the phase difference between filtered intracellular recordings and LFPs, with 0° indicating an in-phase relationship between intracellular voltage and LFP.

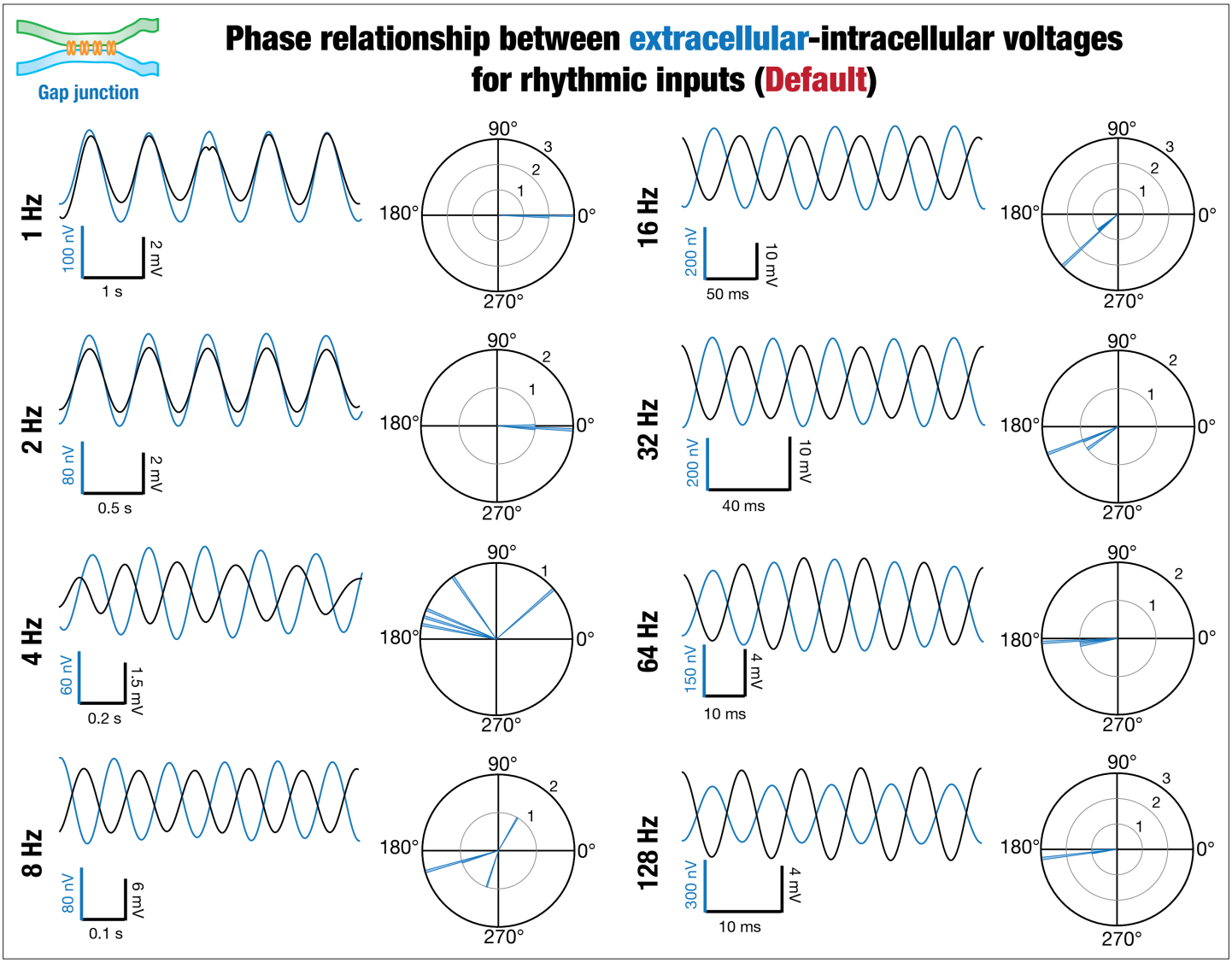


**Figure 8—figure supplement 4.** Somatic intracellular voltage–local field potential (LFP) phase relationship associated with active dendrites receiving rhythmic inputs at various frequencies through gap junctions. Phase difference between filtered somatic intracellular potentials (from ***Figure 7—figure supplement 1***) and corresponding extracellular potentials at different frequencies (1–128 Hz). The following organization is used for each of the eight frequencies. *Column 1:* Example traces of five cycles each of intracellular potential (black) and corresponding LFP (blue). *Column 2:* Polar plots showing the phase difference between filtered intracellular recordings and LFPs, with 0° indicating an in-phase relationship between intracellular voltage and LFP.

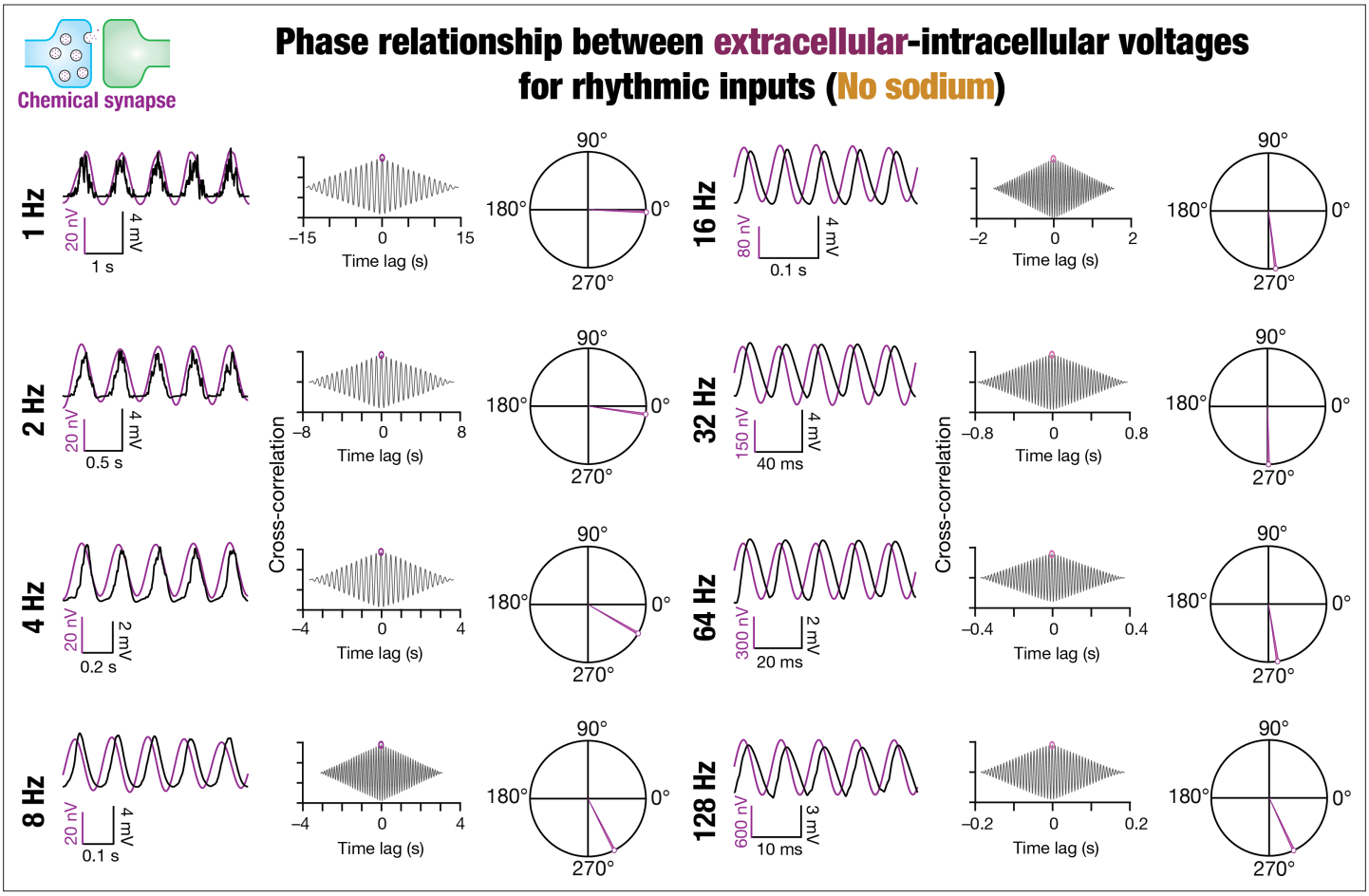


**Figure 8—figure supplement 5.** Somatic intracellular voltage–local field potential (LFP) phase relationship associated with active dendrites receiving rhythmic inputs at various frequencies through chemical synapses in models with no sodium channels. Traces and plots showing phase difference between somatic intracellular potentials (in the absence of sodium conductance) and corresponding extracellular potentials at different frequencies (1–128 Hz). The following organization is used for each of the eight frequencies. *Column 1:* Example traces of 5 cycles each of intracellular potential (black) and corresponding LFP (magenta). *Column 2:* Cross-correlogram between these waveforms, highlighting the peak value with a magenta circle. *Column 3:* Polar plots showing the phase difference between intracellular recordings and LFPs, with 0° indicating an in-phase relationship between intracellular voltage and LFP.

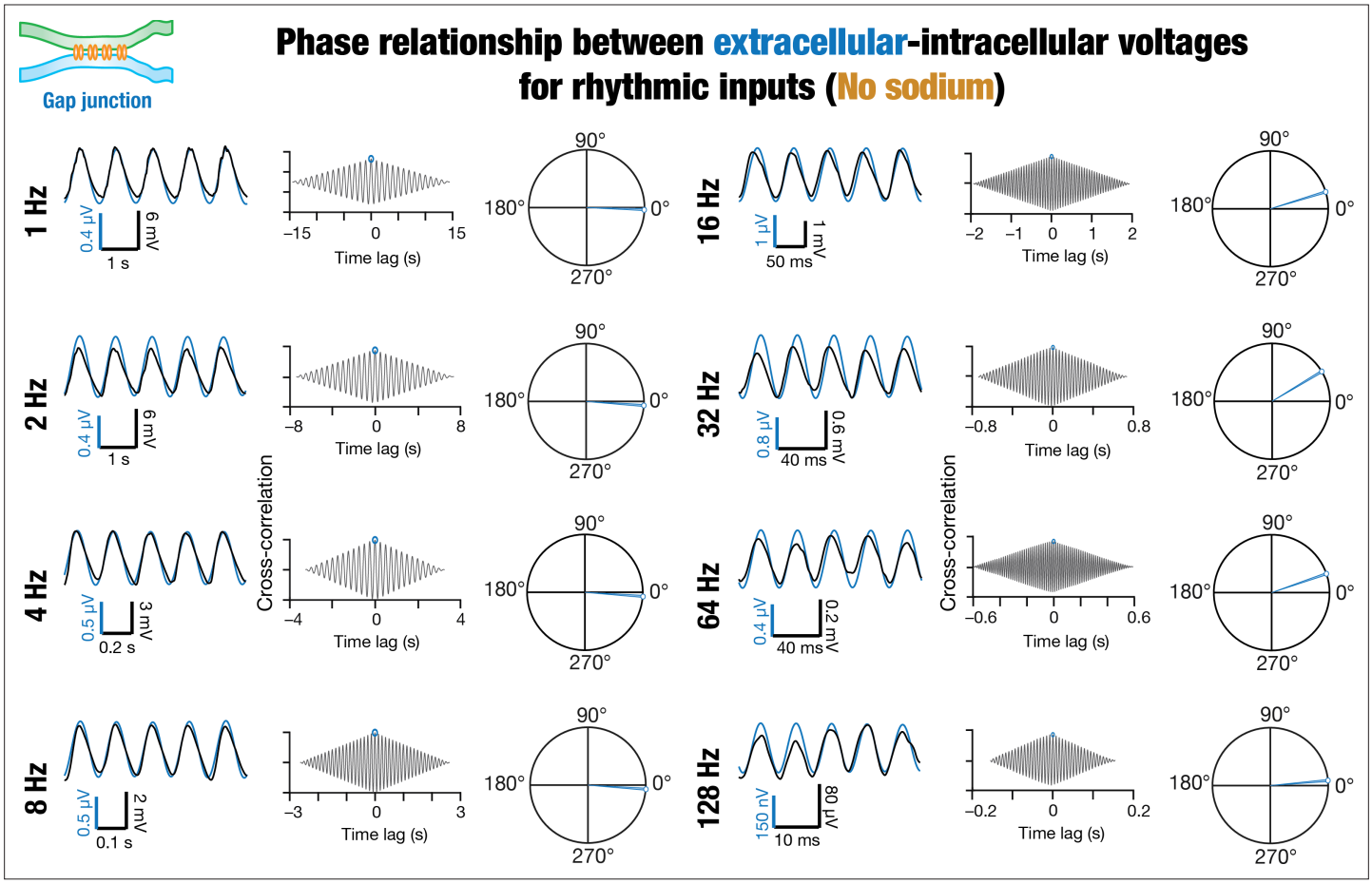


**Figure 8—figure supplement 6.** Somatic intracellular voltage–local field potential (LFP) phase relationship associated with active dendrites receiving rhythmic inputs at various frequencies through gap junctions in models with no sodium channels. Traces and plots showing phase difference between somatic intracellular potentials (in the absence of sodium conductance) and corresponding extracellular potentials at different frequencies (1–128 Hz). The following organization is used for each of the eight frequencies. *Column 1:* Example traces of five cycles each of intracellular potential (black) and corresponding LFP (blue). *Column 2:* Cross-correlogram between these waveforms, highlighting the peak value with a blue circle. *Column 3:* Polar plots showing the phase difference between intracellular recordings and LFPs, with 0° indicating an in-phase relationship between intracellular voltage and LFP.